This is to certify that the

thesis entitled

LOCAL DETERMINATION OF TOOL WEAR
DURING TURNING OPERATIONS

presented by

BULENT DOGRUYOL

has been accepted towards fulfillment
of the requirements for

MS degree in Mechanics

John F. Martin
Major professor

Date 8/8/85

O-7639

LOCAL DETERMINATION OF TOOL WEAR

DURING TURNING OPERATIONS

By

Bulent Dogruyol

A THESIS

Submitted to
Michigan State University
in partial fulfillment of the requirements
for the degree of

MASTER OF SCIENCE

Department of Metallurgy, Mechanics and Materials Science

1985

ABSTRACT

LOCAL DETERMINATION OF TOOL WEAR
DURING TURNING OPERATIONS

By

Bulent Dogruyol

A cutting tool that was instrumented with strain gages was used to machine a low carbon steel. From the measured strains, the cutting forces at the tool tip were calculated. These forces were input into a finite element analysis that was employed to determine the stresses throughout the tool. During machining the tool was periodically examined in a scanning electron microscope to investigate the wear behavior. It was possible to correlate the stresses and forces on the tool with its wear.

ACKNOWLEDGEMENTS

I would like to express my sincere gratitude to Professor John F. Martin for his support and guidance throughout this project. Thanks are also due to Dr. Karen Baker from the Center for Electron Optics for her help concerning the electron microscopy aspects.

TABLE OF CONTENTS

LIST OF TABLES

LIST OF FIGURES

1. INTRODUCTION

Despite the complicated nature of the many interacting parameters in a machining environment, it is the behavior of a very small volume of metal around the cutting edge that determines the performance of tools. During any cutting operation, the interface between tool and work material is largely inaccessible to observation. However, indirect evidence concerning stresses, temperatures and chip formation can be obtained. This study will attempt to evaluate the tool wear and the cutting forces in the case of a turning operation by monitoring the parameters while the process is in progress. The outline that it will follow is shown in the following diagram and can be divided into three parts:

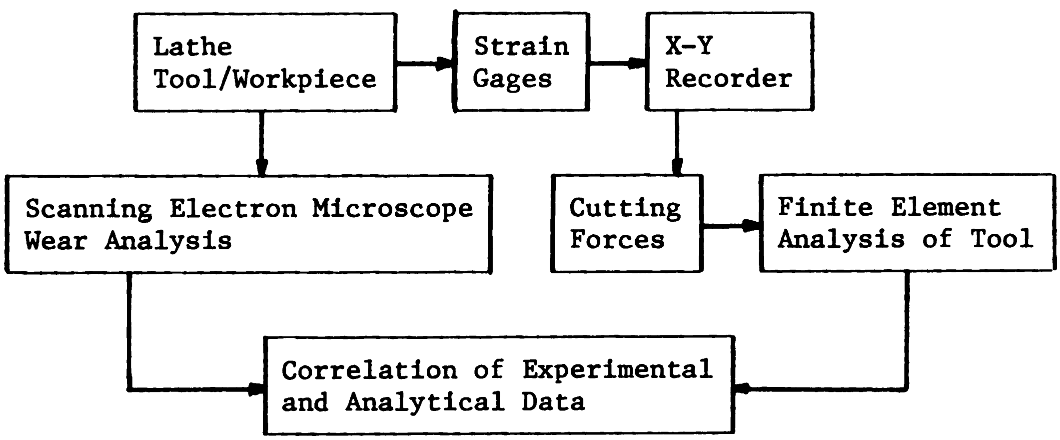

Experimental Techniques: Machining experiments to evaluate the cutting forces that will eventually dull the cutting tool completely. Since the final goal of this work is to correlate wear behavior of the tool with cutting forces, the machining parameters were selected so as to guarantee the gradual wearing and final destruction of the tool.

Analytical Procedures	:	Determination of cutting forces and finite element analysis to evaluate the stress and strain state throughout the cutting tool.
Electron Microscopic Investigations	:	Use of a scanning electron microscope for analysis of wear on the cutting edge of the tool.

2. EXPERIMENTAL TECHNIQUES

2.1. Experimental Setup and its Elements

The experimental part of this thesis consists of a single set of turning operations on a lathe.Strain gages were mounted on three sides near the nose of the tool. These gages were placed in positions such that the forces on the tool tip could be calculated directly using simple beam theory. They were used to continuously measure the strains experienced by the cutting tool during the cutting passes and these strain values were recorded with two X-Y recorders. These measured strains, then, became the input into the beam theory to determine the cutting forces. The elements of this setup are shown in Figure 1.

2.1.1. The Lathe

The experiments were performed on an 8-speed, 13-inch South Bend engine lathe with the following characteristics:

Chuck	: 9 in. with 3 jaws
Spindle speed range	: 30-685 RPM
Bar capacity	: 1 in.

2.1.2. The Workpiece

A low carbon steel, SAE-AISI 1018, was used as the workpiece material to ensure low temperatures near the tool tip where the strain gages were located. SAE-AISI 1018 is a very common material and this

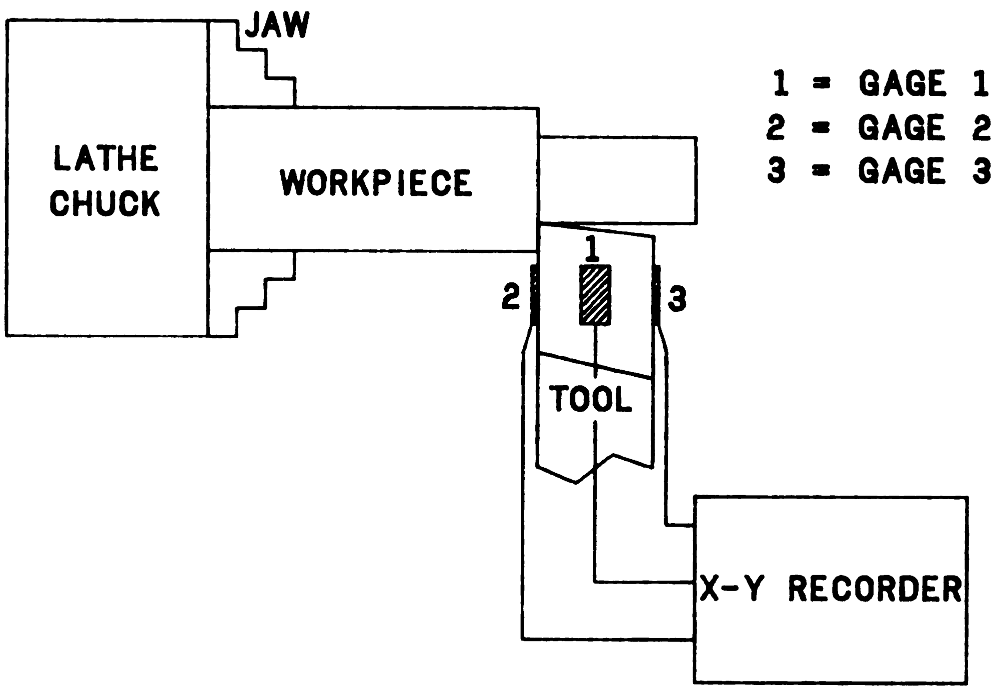

Figure 1. Experimental Setup and its Elements

was a further criterion in selecting the workpiece material. The specimens were cut from cold drawn bar stock with a diameter of 1.0 in. and were 7 in. long. Table 1 summarizes the chemical and mechanical properties of the workpiece material (1,2):

Table 1. Chemical and Mechanical Properties of the Workpiece Material

SAE-AISI Number	C (%)	Mn (%)	P (%) max	S (%) max	Tensile Strength (psi)	Yield Strength (psi)	Elongation (% 2 in.)
1018	.18	.60	.04	.05	68,000	55,000	32.0

Reduction of Area (%)	Hardness BHN	RB
66.5	137	77

2.1.3. The Tool

A high speed steel (HSS) of type M2 (2) was chosen as the cutting tool. This material constitutes a good compromise between strength at high temperature and the toughness requirements for machining relatively soft steels like SAE-AISI 1018. These tools are now the most commonly used of the high speed steels, because they make possible the cutting of steel and other high melting-point materials at much higher rates of metal removal than can be achieved with carbon steel tools. The improved performance is made possible by their retention of hardness and compressive strength to higher temperatures. The composition and hardness of the tool material is given in Table 2 (1,2,3):

Table 2. Chemical Composition and Hardness of the Tool Material

SAE-AISI Number	C (%)	Mn (%)	W (%)	Mo (%)	Cr (%)	V (%)	Fe (%)	Hardness HV	Hardness RC
M2	.85	.30	6.0	5.0	4.0	2.0	Balance	840	65

To enable an uncomplicated 3-D modeling of the tool for the finite element analysis, a simple geometry was desirable; yet it had to be sophisticated enough to machine the workpiece and simulate some actual machine shop conditions. Finally its overall length was kept less than three inches to facilitate its fitting into the specimen chamber of the scanning electron microscope that was used to investigate the wear patterns on the tool tip. Figures 2 and 3 show the geometry of the tool used in these experiments and of a conventional tool geometry that is used in machine shops. The list of various angles comprising the tool geometry is called the "signature" and has been standardized by the American Standards Association. In accordance with the above considerations, the cutting tool employed in this study was ground to the following geometry (1,2,3,4);

		Experimental Tool	Recommended Geometry
Back Rake Angle	=	0	(10)
Side Rake Angle	=	0	(12)
End Relief Angle	=	10	(8)
Side Relief Angle	=	10	(8)
End Cutting Edge Angle	=	10	(8)
Side Cutting Edge Angle	=	0	(15)
Nose Radius	=	1/64 in.	(1/32 in.)

The numbers in parantheses indicate the recommended angles for single

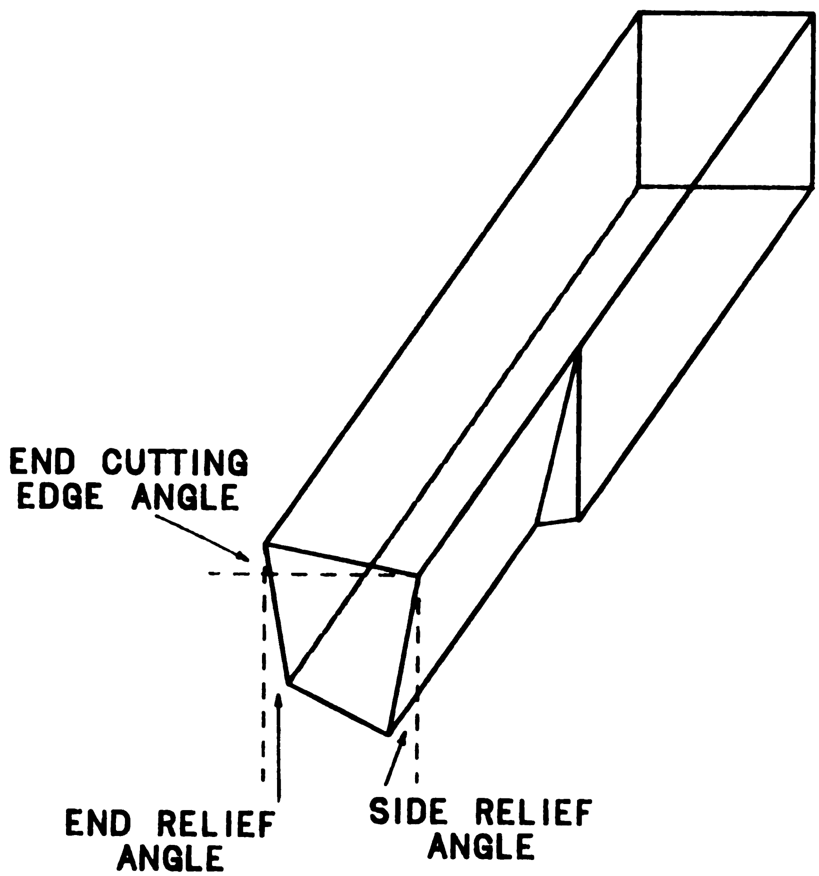

Figure 2. Geometry of the Tool Used in Experiments

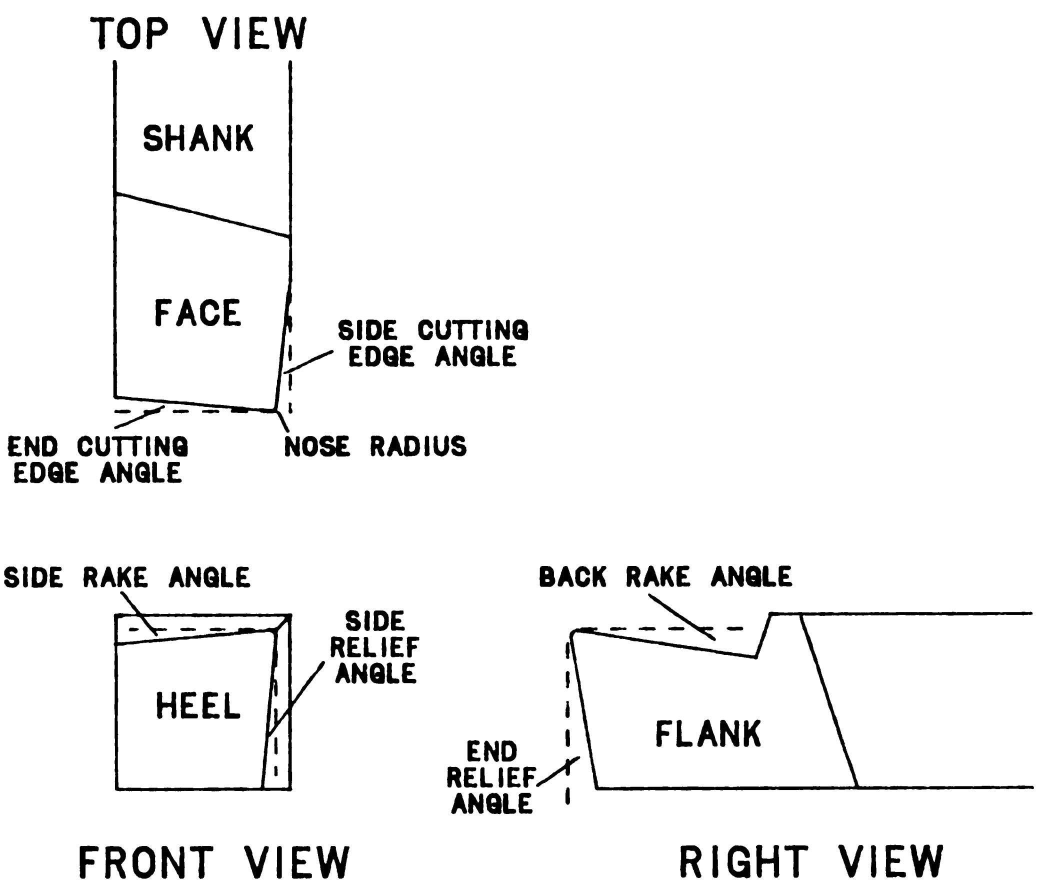

Figure 3. Geometry Definitions of a Conventional Tool

point HSS tools when machining plain low carbon steel.

The deviations of the back rake, side rake and side cutting edge angles from the recommended values will all result in an increased cutting force, decreased tool life and worsened surface finish. These effects, besides the goal of a simplified geometry, were also intended to accelerate the wearing of the tool and to eventually result in failure.

2.1.4. The Strain Gages

Three strain gages, as shown in Figure 4, were mounted on three faces of the tool to monitor the strain state caused by the forces Fx, Fy and Fz. The main purpose of measuring the strains was to use them in determining the cutting forces Fx, Fy and Fz at the tool tip.
Gage 1 was placed on the neutral axis and far enough away from the tip so as to not be affected by the high temperature that develops in the vicinity of the tool tip. Gage 2 was located along the neutral axis of the flank face and gage 3 was placed off the neutral axis and at the lower edge of the right face. All three gages had the same perpendicular distance to the tip (Figure 4). By this configuration the forces Fx, Fy and Fz at the tip can be determined by simple beam theory.
The specifications of the gages are listed below:

Manufacturer: Micro-Measurements
Gage Type : EA-06-075AA-120
Resistance : 120.0 (+/-) 0.15% ohms
Gage Factor : 2.005 (+/-) 0.5% at 75 F.

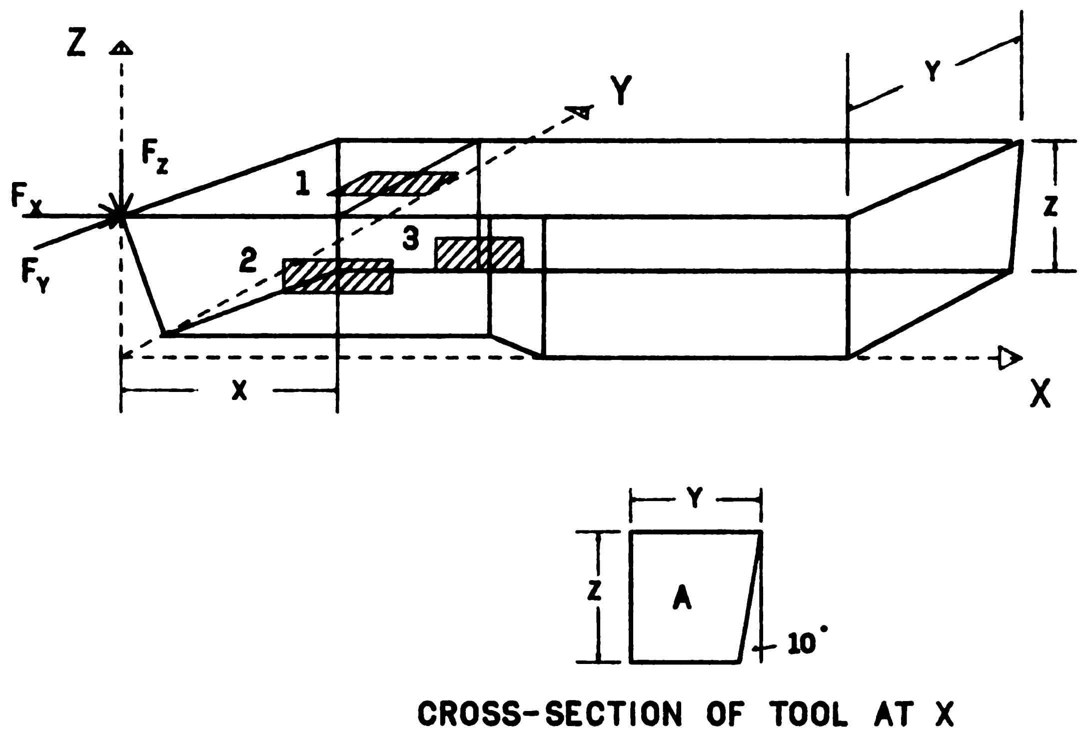

Figure 4. Strain Gages and Cutting Forces

2.2 Experimental Procedure

The machining experiments were carried out on round bar workpieces that were 5.5 in. long which allowed for a cutting time of 60 sec. for each cutting pass at a feed rate of .012 inches per revolution (ipr). At the end of each pass the tool was disengaged, the workpiece was replaced with a new bar with the same diameter and a new pass was started. On one hand, this gave the tool enough time to cool down, thus avoiding the temperature distortion of strain gage readings; on the other hand, the method is not a realistic simulation of continuous cutting operations under shop conditions where the tool remains in contact with the workpiece for longer periods of time. To be in line with the recommended values of cutting speeds and cutting depths when turning low carbon steels, the following values were decided on:

Cutting depth d=0.10 in.

Cutting speed v=118 surface-feet per minute (sfpm)

The magnitude of the cutting speed was obtained by:

v = II*D*N/12	where	D=1 in.	workpiece diameter
		N=450 RPM	spindle speed

The experiments were performed dry.

2.3. Experimental Results

During each cutting pass, two X-Y recorders simultaneously plotted the output from the three strain gages. Altogether 30 passes of 60 sec. duration were carried out on 30 bars resulting in a cumulative cutting time of 30 min. for the tool.

Figure 5 shows the original data trace of strain vs time for one pass. The rapid initial increase in strain for gages 1 and 2 was due to the sudden engagement of the tool with the workpiece. A sudden jump in strains in gage 1 can also occur if a hot chip hits this gage, as indicated in Figure 5. Table 3 shows the average strains obtained from the gages for each pass. Since the strain gradient within a 60 sec pass was small, the table contains the median values measured at the 30 sec. period for each pass. From the strain table, it can be observed that gages 1 and 2 are in tension whereas gage 3 is in compression.This situation is expected since the effect of the larger forces Fz and Fy would produce tensile strains on gages 1 and 2 and compressive strains on gage 3. The strain readings also indicate that during the first half of tool life (first 15 passes) the deformations in the tool increase linearly and slowly. This trend changes in the second half of the tool life (last 15 passes) when the strains rise progressively in an exponen tial manner meaning a corresponding increase in the forces acting at the tool tip. A plot of these data is shown in Figure 6.

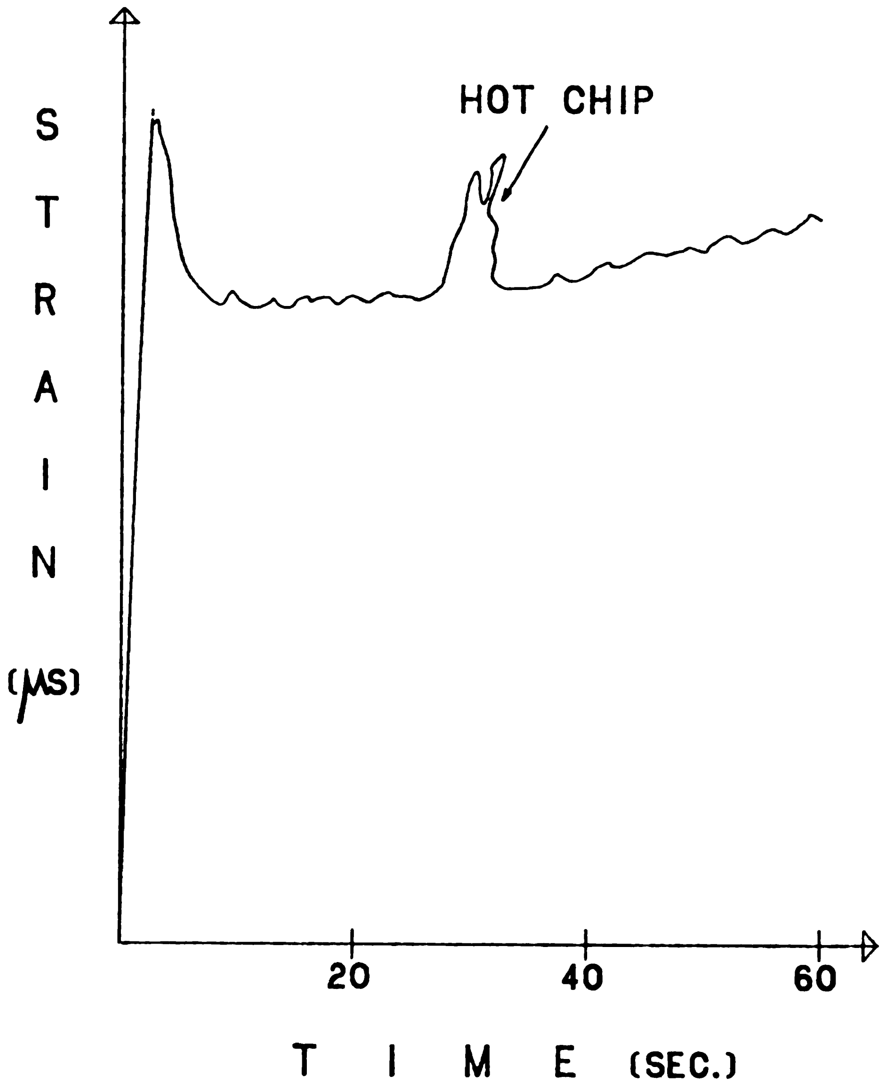

Figure 5. Strain vs Time for One Pass

Table 3. Strain Readings

Workpiece	: SAE-AISI 1018	Feed	: .012 ipr
Tool	: HSS-M2	Cutting depth	: .10 in.
Speed	: 118 sfpm	Duration of each pass	: 60 sec.

Pass	Strain (Microstrains)		
	e1	e2	e3
1	187	143	-246
2	188	145	-248
3	190	147	-250
4	192	149	-252
5	194	152	-255
6	195	153	-256
7	196	154	-257
8	198	155	-258
9	200	157	-259
10	202	159	-261
11	203	160	-262
12	204	161	-263
13	205	162	-265
14	206	163	-267
15	208	165	-269
16	210	167	-271
17	212	169	-274
18	215	172	-277
19	218	175	-281
20	222	179	-285
21	226	181	-288
22	231	183	-292
23	236	186	-297
24	242	190	-302
25	249	194	-307
26	256	201	-319
27	266	209	-334
28	278	218	-349
29	294	227	-360
30	321	241	-379

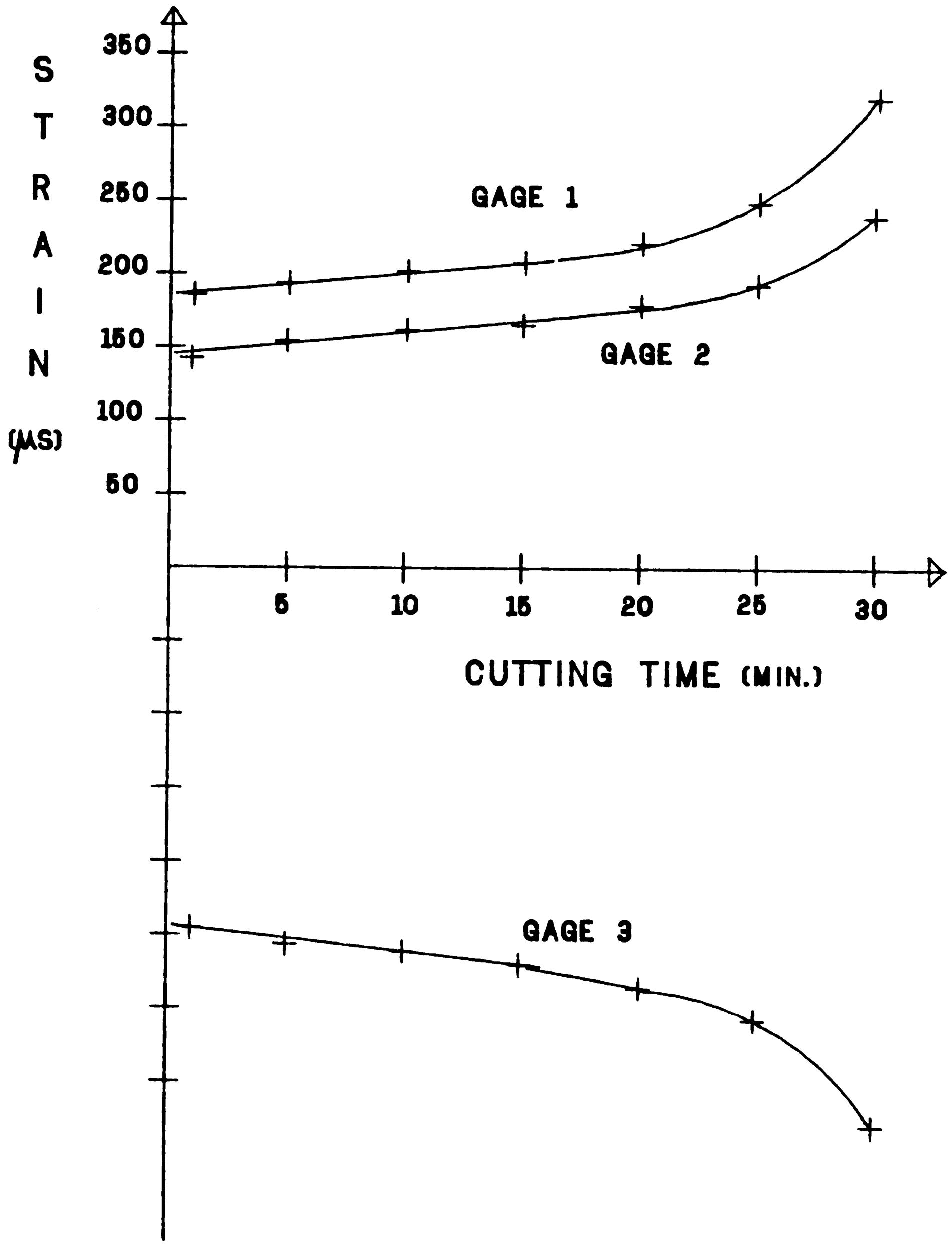

Figure 6. Strain vs Cumulative Cutting Time

3. ANALYTICAL PROCEDURES

3.1. Calculation of Cutting Forces

By using simple beam theory the forces at the tool tip that corresponded to each strain state were calculated. Fz is the tangential cutting force due to rotational relative motion between the tool tip and the workpiece. This is normally the largest cutting force component and acts in the direction of the cutting velocity. Fy, the feed force, is generated by the longitudinal feeding motion of the tool with respect to the workpiece. The magnitude of Fy, in general, ranges between 30% and 60% of Fz. Fx, the radial force, is the least significant of all cutting force components and is produced by the thrusting action of the tool tip against the work material. Usually this force,Fx is neglected for the purposes of analysis of cutting forces in simple turning (5,6,7).

A summary of the beam theory employed for this analysis is given as follows:

<u>Strains on Gage 1</u>

Compression due to Fx: $S_1 = -\frac{Fx}{A} = E\ e_1$ thus $e_1 = -\frac{Fx}{E\ A}$

Bending due to Fy : $e_1 = 0$ gage on neutral axis

Bending due to Fz : $S_1 = \frac{M\ c}{I} = \frac{Fz\ (x)\ z/2}{(1/12)\ z^3\ y} = E\ e_1$

$$\text{thus}\quad e_1 = \frac{6\ x}{E\ z^2\ y}\ Fz$$

Strains on Gage 2

Compression due to Fx: $S_2 = -\frac{Fx}{A} = E\,e_2$ thus $e_2 = -\frac{Fx}{E\,A}$

Bending due to Fy : $S_2 = \frac{M\,c}{I} = \frac{Fy\,(x)\,y/2}{(1/12)\,y^3\,z} = E\,e_2$

thus $e_2 = \frac{6\,x}{E\,y^2\,z}\,Fy$

Bending due to Fz : $e_2 = 0$ gage on neutral axis

Strains on Gage 3

Compression due to Fx: $S_3 = -\frac{Fx}{A} = E\,e_3$ thus $e_3 = -\frac{Fx}{E\,A}$

Bending due to Fy : $S_3 = -\frac{M\,c}{I} = -\frac{Fy\,(x)\,y/2}{(1/12)\,y^3\,z} = E\,e_3$

thus $e_3 = -\frac{6\,x}{E\,y^2\,z}\,Fy$

Bending due to Fz : $S_3 = -\frac{M\,c}{I} = -\frac{Fz\,(x)\,z/2}{(1/12)\,z^3\,y} = E\,e_3$

thus $e_3 = -\frac{6\,x}{E\,z^2\,y}\,Fz$

Linearly adding strains for each gage results in:

$$e_1 = -\frac{Fx}{E\,A} + \qquad + \frac{6\,x}{E\,z^2\,y}\,Fz$$

$$e_2 = -\frac{Fx}{E\,A} + \frac{6\,x}{E\,y^2\,z}\,Fy$$

$$e_3 = -\frac{Fx}{E\,A} - \frac{6\,x}{E\,y^2\,z}\,Fy - \frac{6\,x}{E\,z^2\,y}\,Fz$$

Solving for Fx, Fy and Fz:

$$Fx = -\frac{E\,A}{3}\,(e_1 + e_2 + e_3)$$

$$Fy = \frac{E\,y^2\,z}{18\,x}\,(-\,e_1 + 2e_2 - e_3)$$

$$Fz = \frac{E}{18}\frac{z^2 y}{x} \; (2e_1 - e_2 - e_3)$$

With $x = .250$ in.
$y = .500$ in.
$z = .500$ in.
$A = .228\ in^2$
$E = 30x10^6$ psi. (see Figure 4)

one obtains:

$$Fx = 2.2800x10^6 \; (e_1 + e_2 + e_3)$$

$$Fy = 0.8333x10^6 \; (-e_1 + 2e_2 - e_3)$$

$$Fz = 0.8333x10^6 \; (2e_1 - e_2 - e_3)$$

Based on this analysis, the values of the cutting forces at each pass are given in Table 4. A plot of these data is presented in Figure 7. On this plot also the most striking feature of cutting force behavior with respect to cutting time is the rapid exponential increase in cutting forces in the last one third of the accumulated cutting time. Within the first two thirds of cutting time (first 20 min.), the rise in cutting forces is linear with a shallow slope; in fact, the tangential cutting force increases only by 15% within this time period. However, the increase within the last 10 min. amounts to a total of 42% increase over the starting value. This pattern is not a result of a variation in cutting parameters since they were all kept constant. The increase in these forces can be attributed to the changes in geometry and cutting conditions which resulted from wear in the tool/work contact area as well as an increase in temperature.

A comparison of the magnitudes of feed and tangential cutting forces shows that the feed force has a relatively high value, i.e. above 70% of Fz throughout 30 min. This is indicative of a large

Table 4. Calculated Cutting Forces at the Tool Tip

Pass	Fz (lb)	Fy (lb)	Fx (lb)
1	398	287	-192
2	399	292	-194
3	402	295	-198
4	406	298	-203
5	409	304	-207
6	411	306	-210
7	413	308	-212
8	416	309	-219
9	418	311	-223
10	421	314	-228
11	423	316	-230
12	425	318	-231
13	427	320	-232
14	430	323	-233
15	433	326	-237
16	437	329	-241
17	441	333	-244
18	446	338	-251
19	452	344	-255
20	458	351	-264
21	466	353	-271
22	476	356	-278
23	486	361	-285
24	497	367	-296
25	509	372	-310
26	525	388	-315
27	548	405	-321
28	573	422	-335
29	601	433	-367
30	649	452	-419

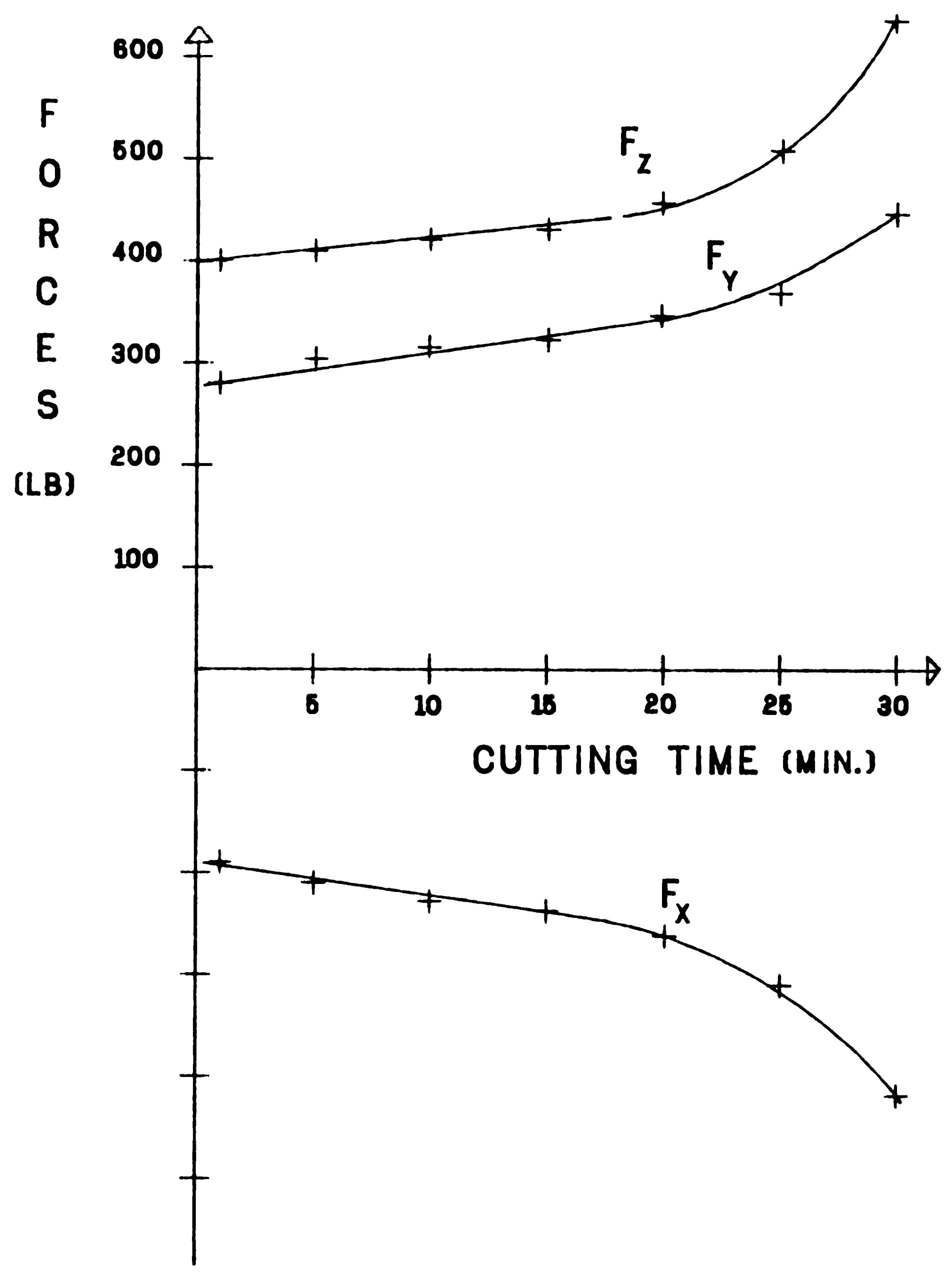

Figure 7. Cutting Forces vs Cumulative Cutting Time

chip/tool contact area on the rake face(see Figure 14), since the feed force is a measure of the drag which the chip exerts as it flows away from the cutting edge across the rake face (5,6). The analysis produces negative values for the radial force Fx which means that it is acting away from the tool tip in a radial direction as a tensile force. This is not realistic. However, this effect might have been caused due to extensive deformation into the workpiece of the cutting edge under high tangential and feed forces causing the gages to interpret the radial force as being tensile (see Figure 8). This and all other aforementioned effects will be discussed in more detail when the results of the electron microscopic investigations are presented.

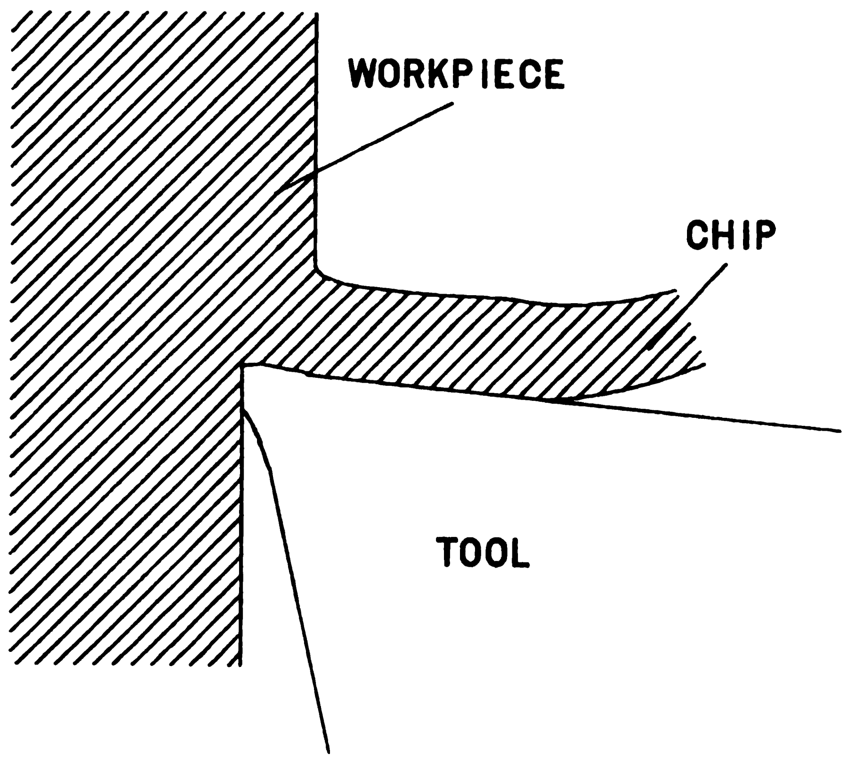

Figure 8. Deformation of the Cutting Edge Under Compressive Stress

3.2. Finite Element Analysis

A finite element model of the tool was used to obtain an estimation of stresses acting throughout the tool. The input to the analysis, which used the commercially available software package ANSYS by Swanson Analysis Systems, Inc. (8), was the cutting forces calculated in the previous section.

3.2.1. The Tool Model

Since the idea was to obtain a rough estimate of stresses, a relatively coarse mesh was used and the tool tip was approximated as a point. Although it was expected that this approximation will result in higher theoretical stresses than actual, it simplified the mesh generation scheme a great deal enabling partial automatic mesh generation in the preprocessing phase. The element employed in the analysis was a 3-D isoparametric stress solid element STIF45. It is used for three dimensional modeling of solid structures and is defined by eight nodal points having three degrees of freedom at each node (translations in the nodal x, y and z directions). A further advantage of tool nose approximation as a point lies in the fact that it was possible to select an eight node volume element rather than a higher order, nonlinear volume element, i.e. 16- or 20-node elements (8). The effect was a reduction in the degrees of freedom which decreased the solution core size and the running time. This element is shown in Figure 9. The resulting tool model consisted of 100 elements and 180 nodes (see Figure 10). In the analysis, the cutting tool was treated as a cantilever beam

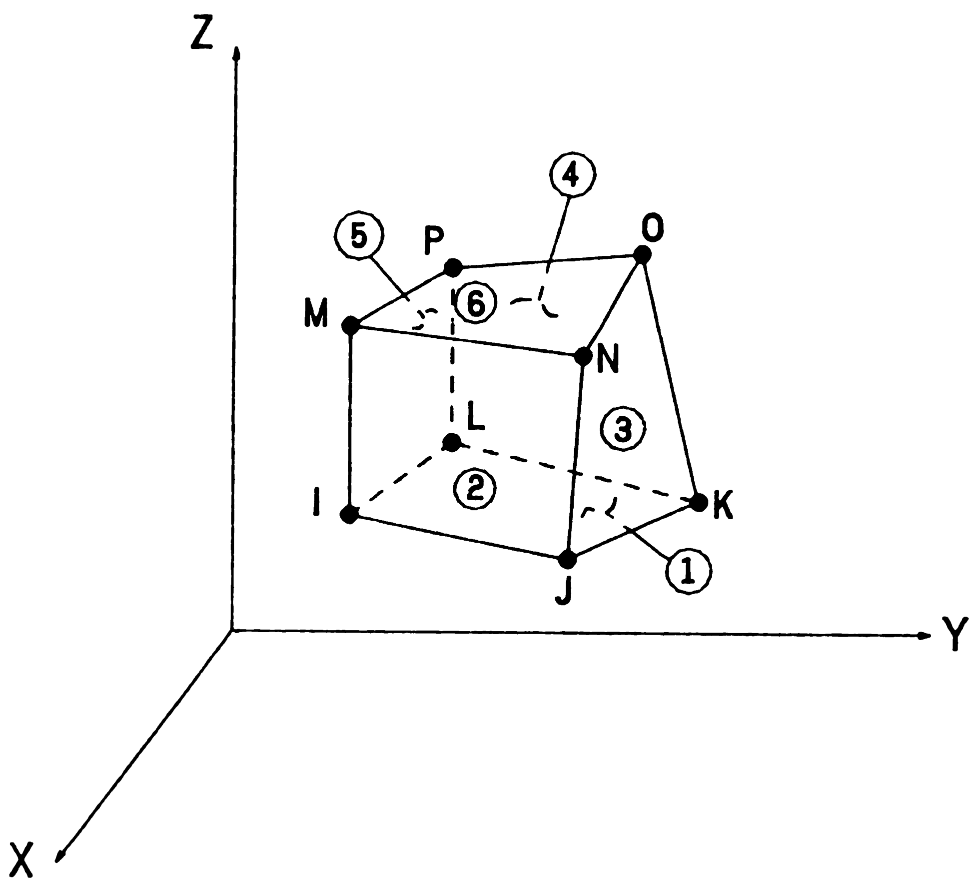

Figure 9. 3-D Isoparametric Element

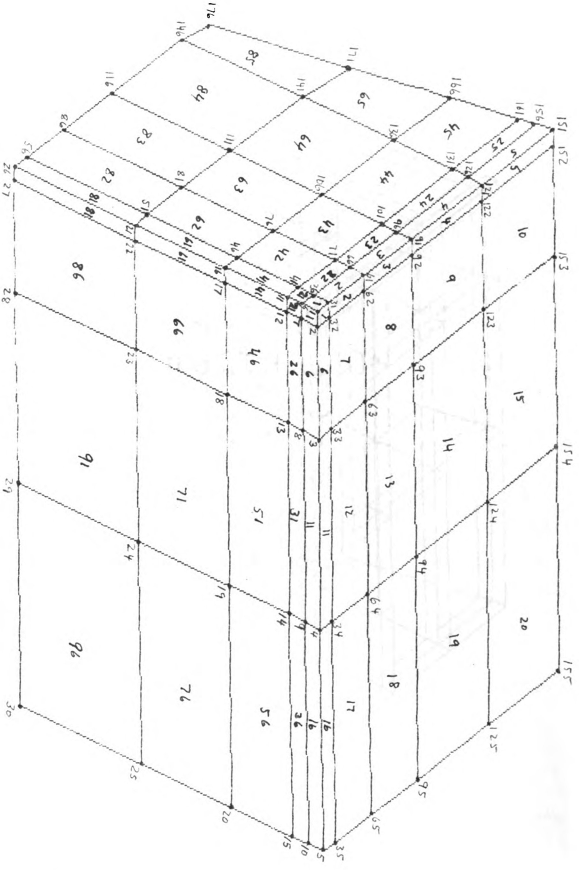

Figure 10. Finite Element Model of the Tool

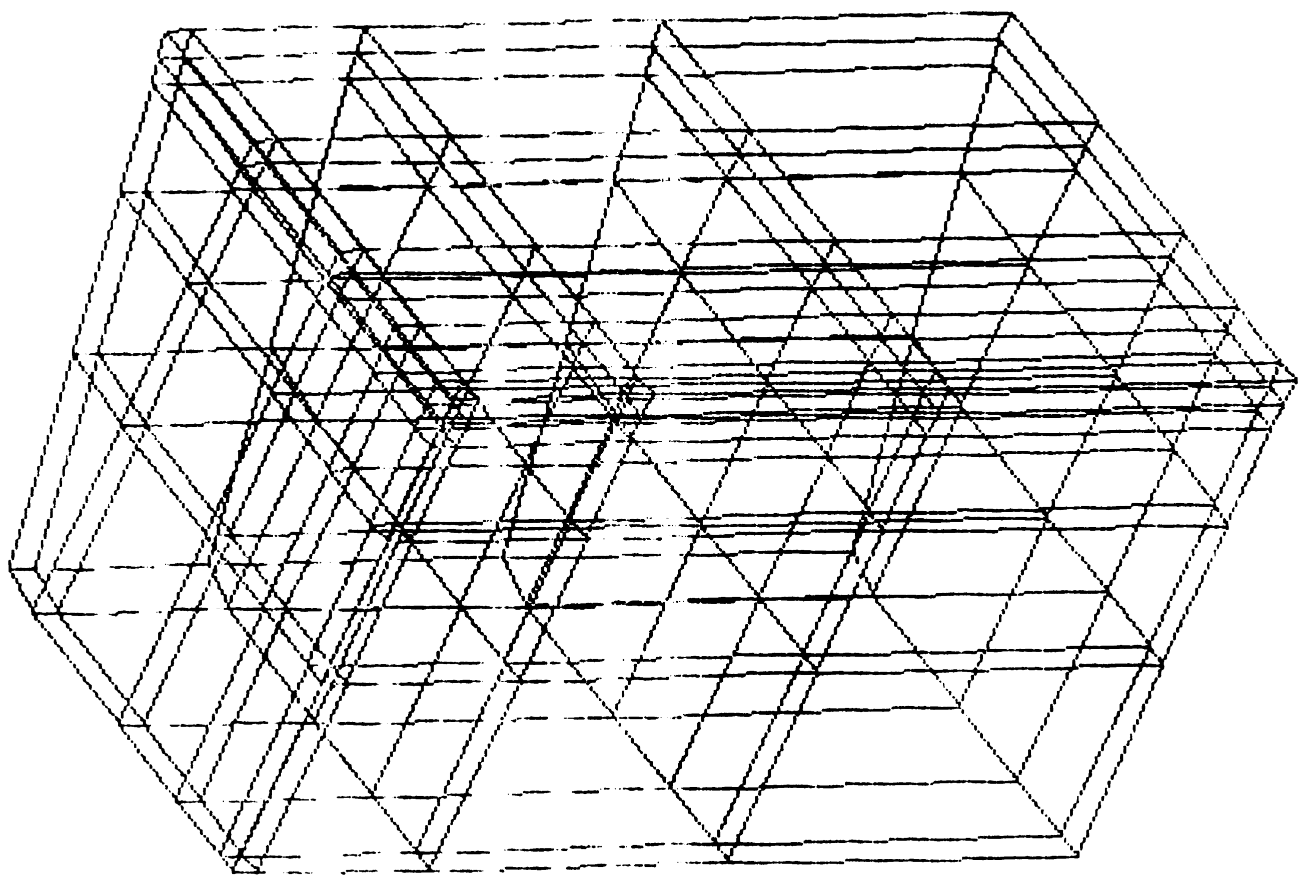

Figure 10. Finite Element Model of the Tool

clamped within the tool holder. Consistent with this situation, all three degrees of freedom for all the dodes at this end of the tool were set to zero. The input to the program consisted of the cutting forces at different times during the tool life.

3.2.2. Stress Distribution in the Tool

The cutting force acting on a tool with a small rake angle imposes a stress on the rake face which is largely compressive in character. The mean value of this stress is determined by dividing the cutting force by the contact area, which in reality is very difficult to determine accurately. In a lathe, where the tool acts as a cantilever, there are also bending stresses giving tension on the upper surface between the contact area and the tool holder. These stresses are negligible at the tool tip, because they rise linearly starting at the tip and reach a maximum at the clamped end of the tool. The tool model described above was used to calculate the compressive stresses close to the tool tip by feeding the program with the cutting forces after cutting times of 1 min., 5 min., 10 min., 15 min., 20 min., 25 min., 28 min., and at the end of the tool life of 30 min. Table 5 lists these values:

Table 5. Compressive Stresses at the Cutting Edge

Cutting Time (min.)	Compressive Stress (psi.)
1	13,650
5	15,750
10	18,900
15	22,200
20	28,450
25	36,300
28	42,350
30	48,350

These values, as plotted in Figure 11, are the compressive stresses in the first element of the model near the tip and are averaged over the element. This element, being .1 in. by .1 in., has an area of .01 in^2 on the rake face. This area can be, in general, assumed to be larger than the actual chip/tool conatact area whose accurate value usually is not known. But methods have been developed for measuring stress distribution under certain simplified laboratory conditions (5,9,10). They provide evidence that the compressive stress is highest near the cutting edge, diminishing rapidly across the rake face to zero where the chip breaks contact with the tool. It seems probable that this stress distribution is common during cutting and that the compressive stress at the edge is often double the mean stress or even greater. Figure 12 qualitatively illustrates this distribution for the loads after a cutting time of 30 min. Under the above assumptions one would expect stresses to be on the order of 100,000 psi at the cutting edge. This stress then rapidly decreases along the length of the element away from the cutting edge. This situation would be comlicated in the presence of a built-up edge in which case the stresses would probably be lower.

The very high normal stress levels account for the conditions of seizure on the rake face, particularly near the cutting edge. The conditions of seizure will be discussed in the next section. If a tool does not possess adequate strength, it may undergo local plastic deformation and subsequent cyclic softening under these conditions. The tool used in these experiments had a yield strength of approximately 147,000 psi. It is very likely that this tool at least was

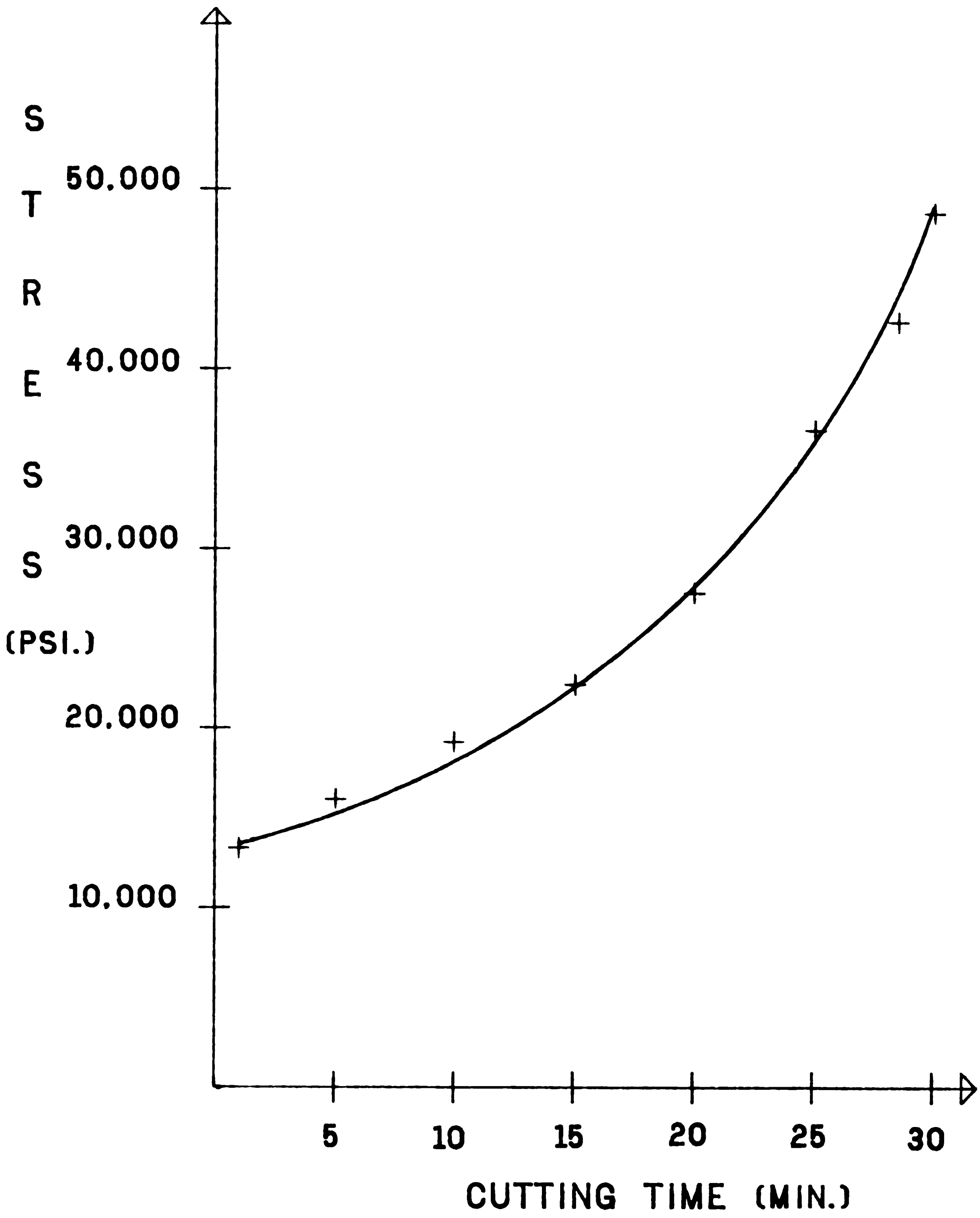

Figure 11. Comressive Stress vs Cumulative Cutting Time

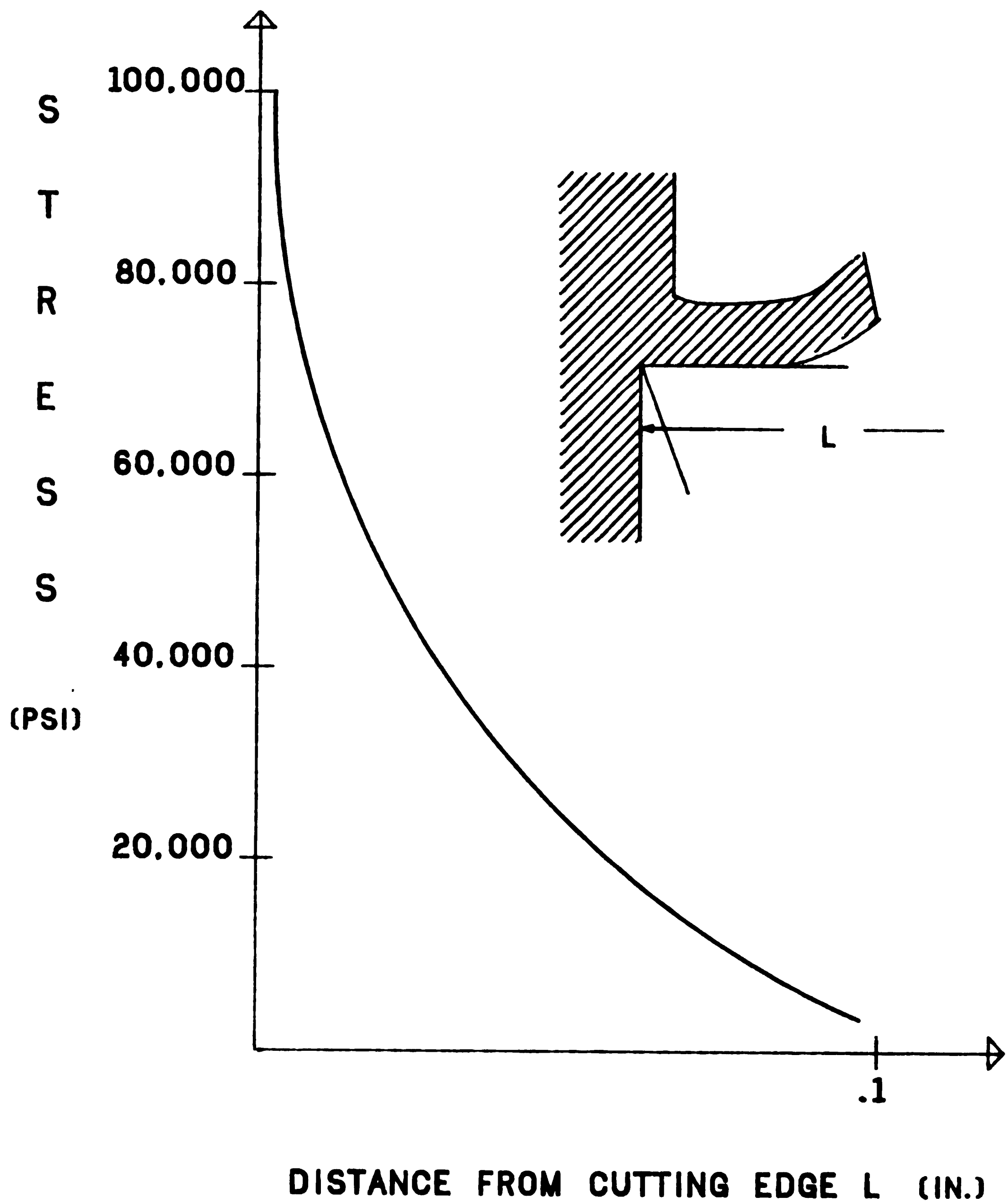

Figure 12. Compressive Stress Distribution on the Rake Face

subjected to large elastic deformation locally which means a change in predefined geometry. This would affect the cutting performance.

The graph of stress vs cutting time reveals similar trends as indicated by strain vs time and force vs time diagrams. Again the stress at the cutting edge increases progressively with increasing cutting time (Figure 11).

4. ELECTRON MICROSCOPIC INVESTIGATIONS

The machining experiments were periodically stopped to assess the amount and nature of wear at the tool tip. During the course of the 30 min. tool life, the tool was removed several times from its holder and examined in a scanning electron microscope (SEM) for changes of shape. Interruptions were more frequent toward the end of the tool life. The use of an SEM and visual inspection were the only methods employed in this wear study. Before the discussion of the SEM results, as shown in Figures 17-29, is given, an overview of the different wear mechanisms on HSS tools is presented (5,11,12,13,14,15).

4.1. Wear Mechanisms on High Speed Steel Tools

When cutting metals, a tool with the shape of a large-angled wedge is driven asymmetrically into the work material to remove a thin layer (the chip) from a thicker body (the workpiece) (see Figure 13). The chip formation occurs as the work material is sheared in the region of a plane (the shear plane) extending from the tool edge to the position where the upper surface of the chip leaves the work surface (length OD in Figure 13). In this process, the whole volume of metal removed is subjected to extensive plastic deformation, as indicated by the transformation of volume V into V' in Figure 13. The chip thickness t_2 is always larger than the feed t_1, i.e. the chip thickens as it leaves the workpiece along the shear plane due to excessive plastic deformation. The amount of this deformation and therefore of chip thickening is dependent upon the shear plane angle ϕ (see Figure 13).

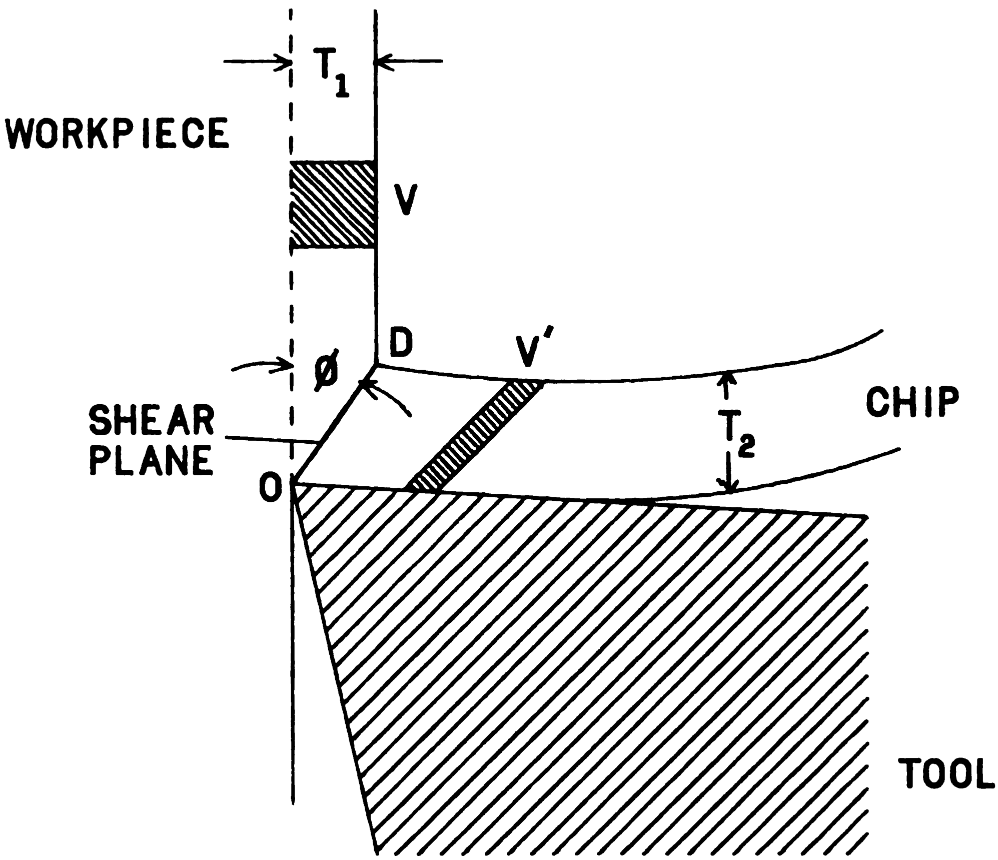

Figure 13. Chip Formation

Deformation and thickening are large at small angles, since the chip is forced to leave the workpiece at a tight curve; they reach an optimum at ϕ = 45 and grow again as ϕ increases.

The wear pattern at the tool/chip interface is significantly determined by the movement of the chip across the rake face and around the tool edge. In most analyses this has been treated as a classical friction situation, in which frictional forces tend to restrain movement across the tool surface with a coefficient of friction between the tool and the work materials as the coupling factor. This approach is inappropriate to most metal cutting conditions. The concepts of friction apply when the stresses between surfaces are small compared with the yield stress of the materials, which is true for many engineering situations. But for most metal cutting operations the contact between tool and the work surfaces is so nearly complete over a large part of the total area of the interface, that sliding at the interface is impossible under most cutting conditions. Under these conditions of seized or interlocked surfaces the movement of work material over the tool surface cannot be adequately described using the terms 'sliding' and 'friction', because the force parallel to the tool surface is not independent of the contact area, but on the contrary, the area of contact between tool and workpiece is a very important parameter in metal cutting. Also, under the conditions of seizure there can be no simple relationship between the fo-ces normal to and parallel to the tool surface as is the case under conditions of sliding. Even under seizure conditions, it is rare that the whole area of contact is seized together. Some frictional sliding occurs in an intermittent contact area (see Figure 14). The relative movement between chip and tool continues under conditions of seizure since the contact area is small and sufficient force is applied (feed force) to shear the work material near the seized interface. Under seizure conditions it can no longer be assumed that relative movement takes place at the interface as is teh case with frictional movement, because the force required to overcome the interlocking and bonding is normally higher than that required to shear the adjacent material. Relative motion under seizure involves bulk shearing in the weaker of the materials.

4.1.1. Plastic Deformation by Shear at High Temperature

The characteristic form of this type of wear is the formation of a crater, a hollow in the rake face some distance behind the cutting edge (see Figure 15). The crater is located at the hottest part of the rake surface from where the hot tool material is sheared since its yield strength is greately lowered at high temperatures. Another factor is the increase in the yield strength of chip material which is subject to high strain rates in the flow zone, thus becoming strong enough to shear layers of tool material from hot regions. This is a rapid acting wear mechanism, forming deep craters, which weaken the cutting edge so that the tool may be fractured.

4.1.2. Plastic Deformation Under Compressive Stress

The compressive stress acting on the rake face is maximum at or close to the cutting edge and when the stress is very high, the tool

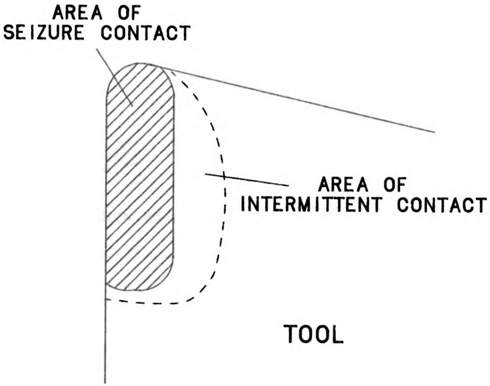

Figure 14. Seizure and Intermittent Contact Ares

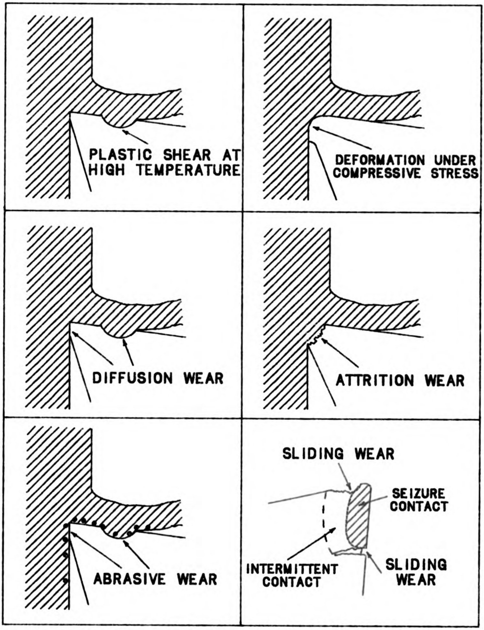

Figure 15. Wear Mechanisms on HSS Tools

edge may be deformed downward (see Figure 15). This is a deformation rather than a wear process, since no tool material is removed, but it results in increased tool forces and brings into play or accelerates wear processes which reduce the life of the tool. This wear mechanism limits also the maximum workpiece hardness which can be machined with HSS tools, since harder materials would cause excessive deformation.

4.1.3. Diffusion Wear

Tools may be worn by metal and carbon atoms from the tool diffusing into and being carried away by the stream of work material flowing over its surface. Rates of diffusion increase rapidly with temperature. With HSS tools used in the usual cutting speed range, rates of wear by diffusion are relatively slow because the interface temperatures are relatively low. Diffusion accounts for the formation of craters at speeds below those at which plastic deformation begins. Above these speeds the damage caused by diffusion wear is obscured by the effect of plastic deformation, which is a much more rapid wear mechanism. Wear by diffusion also depends on a rapid flow rate in the work material very close to the seized surface, to carry away the tool metal atoms.

4.1.4. Attrition Wear

This type of wear is more likely to occur at relatively low cutting speeds where temperatures are low and wear based on plastic shear or diffusion does not occur. The flow of metal past the cutting edge becomes more irregular, less stream-lined or laminar and contact with the tool may be less continuous. Under these conditions larger fragments of microscopic size may be torn intermittently from the tool surface. This is usually a slow form of wear, but more rapid destruction of the tool edge occurs in operations involving interruptions of cut or where vibration is severe due to lack of rigidity in the machine tool or very uneven work surfaces (see Figures 15,24,28).

4.1.5. Abrasive Wear

Abrasive wear of HSS tools requires the presence in the work material of particles harder than the martensitic matrix of the tool. Hard carbides, oxides and nitrides are present in many steels, in cast iron and in nickel-based alloys, but there is little direct experimental evidence to indicate whether abrasion by these particles does play an important role in the wear of tools. Where the work material contains greater concentrations of harder particles, such as pockets of sand on the surface of castings, rapid wear by abrasion undoubtedly occurs. But it seems doubtful whether under conditions of seizure, small, isolated hard particles in the work material can make an important conribution to wear (see Figures 15 and 27).

4.1.6. Wear Under Sliding Conditions

At those parts of the interface where sliding occurs, either continuously or intermittently, other wear mechanisms can come into play. The parts of the surface particularly affected are those shown as areas of intermittent contact (see Figures 15,19 and 23). The wear mechanisms operating in these sliding regions are probably those which occur under more normal engineering conditions at sliding surfaces, involving both abrasion and metal transfer, and greatly influenced by chemical reactions with the surrounding atmosphere.

To summarize, the wear and deformation processes which have been shown to change the shape of the tool and to affect tool life, depend on many factors: the work material, the machining operation, cutting conditions, tool geometry, and the use of lubricants. In general the first three wear mechanisms (4.1.1, 4.1.2, and 4.1.3) are important at high rates of metal removal where temperatures are high and their action is accelerated as cutting speed increases. It is these processes which set the upper limit to the rate of metal removal. At lower speeds, tool life is more often terminated by one of the last three - abrasion, attrition or a sliding wear process - or by fracture.

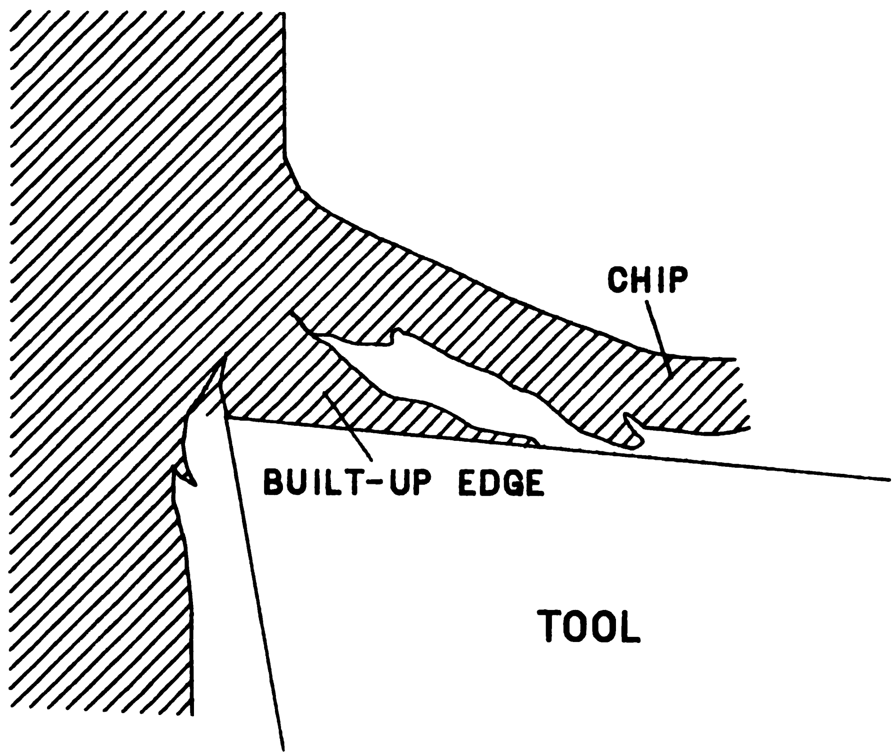

Figure 16. Built-up Edge Formation

4.2. Results of Electron Microscopic Investigations

To monitor the progress of tool wear as a function of cutting time, the tool tip was examined in a scanning electron microscope (SEM). For external examination the SEM is particularly valuable because of its great depth of focus and it was convenient that the entire tool fit into the stage of the microscope.

At first the tool tip remained sound and unharmed. Figure 17 shows the rake face of the tool with the left edge being the side cutting edge. There are no signs of visible wear and the grinding marks are still visible. This picture was taken after 5 min. of cutting. At the end of 10 min. of cutting time, one can detect signs of sliding wear as shown in Figure 18. In this picture of the rake face, the left edge is the side cutting edge and the right edge is the end cutting edge. An indentation due to crossing of the chip across the side cutting edge was forming as shown in the lower left portion of the picture. The frictional rubbing marks between the tool and chip just before the chip leaves the tool face are visible in the lower right quadrant of the picture. These marks also outline the intermittent contact area of the tool/chip interface. Some work material, including a piece of a chip, is shown adhering to the tool along the edge. This picture was taken after 10 min. of cutting. This wear pattern remained stable for a large portion of the remaining tool life. Wear progressed slowly and steadily. Figures 19,20,21 and 22 show the increase in the size of sliding wear marks. This is very evident in Figure 19.

Figue 17. Tool Tip After 5 min. of Cutting

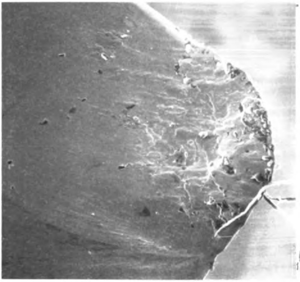

Figure 18. Tool Tip After 10 min. of Cutting

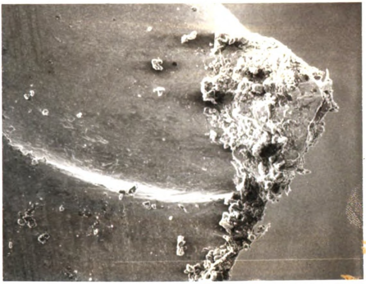

Figure 19. Tool Tip After 20 min. of Cutting

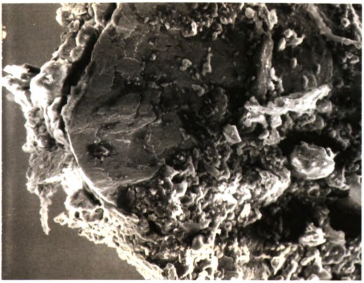

Figure 20. Tool Tip After 20 min. of Cutting (blow-up of Figure 19)

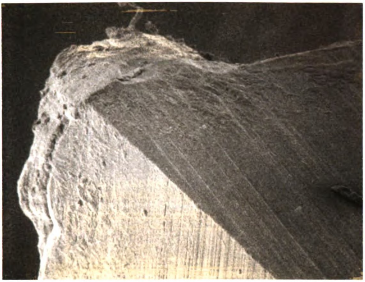

Figure 21. Built-up Edge Adhering to the Rake Face of the Tool

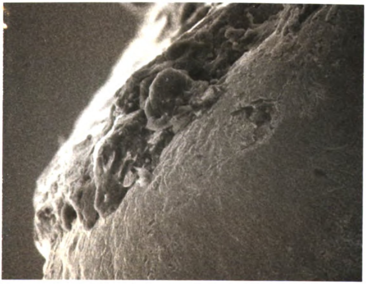

Figure 22. Side Cutting Edge After 24 min. of Cutting

The indentation on the side cutting edge as shown in Figure 19 also extends down the flank face which can be seen in Figure 21. Figure 22 depicts the edge of the tool close to the nose. It is evident that the edge is rounded and chipped in the lower portion. Although it is difficult to exactly classify the type of wear occuring, a combination of abrasive and attrition wear appears likely. These photographs (Figures 19,20,21,22) which were taken after 20 min. to 25 min. cutting times, also display the phenomenon of seizure between work material and the tool. Some degree of metallurgical bonding at the tool/chip interface might have taken place since the contact remained intact during the disengaging of the tool from the workpiece at the end of the cutting pass. There is, however, a considerable variation in the strength of bond generated, since not all pictures display the cutting tool with work material adhering to it. Figures 19,20 and 22 show the ductile tensile fracture of the work material adhering to the tool face. This occured when the tool was seperated from the chip in a tensile fracture mode when the tool was disengaged from the workpiece. As pointed out earlier in the discussion of cutting force magnitudes, the radial force against the nose of the tool did not have a significant effect as is visible in Figures 19 and 20. The nose is still sharp and intact. This is evidenced by the fact that the grinding marks on the flank and end relief face can be followed almost up to the nose (Figure 21). Another important feature of metal cutting operations, the built-up edge, can also be observed in Figure 21 (see also Figure 16). The built-up edge forms under conditions of seizure when work hardened material, adhering around the cutting edge and along the rake face, accumulates to displace the chip from immediate direct contact with the tool. The built-up edge is not a seperate body of metal but forms a continuous body of metal with the chip. Its presence transfers the flow zone, where the relative motion between the chip and tool occurs, to the top of itself. The built-up edge is sheared off and is not observable at higher cutting speeds (5, 6,13,15).

Due to sliding wear the tool material is weakened progressively causing abrasive and attrition wear to take over. Figures 23 and 24 show this effect. The weakening of the nose area in particular is very evident. The rake face is no more smooth, but chipped and cracked due to attrition and abrasion. These pictures were taken after 26 min. of cutting time. Shortly after these pictures were taken the nose of the cutting tool collapsed under machining. Figures 25 and 26 show the tip of the tool with the nose broken off. The effects of attrition on the tool can be seen in Figures 27,28 and 29. Large fragments are being pulled away, leaving a very uneven worn surface. The tool edge is essentially being 'nibbled' away.

Figure 23. Rake Face After 26 min. of Cutting

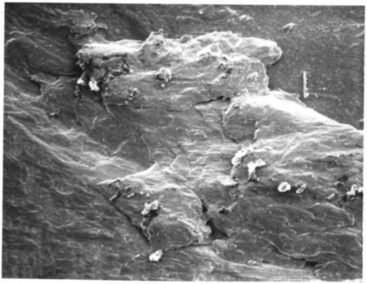

Figure 24. Rake Face After 26 min. of Cutting (blow-up of Figure 23)

Figure 25. Rake Face After 28 min. of Cutting

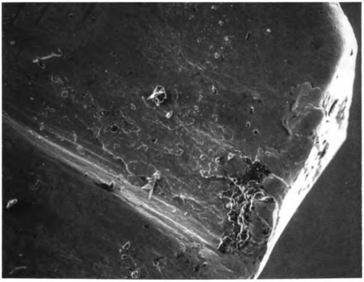

Figure 26. Rake Face After 28 min. of Cutting (blow-up of Figure 25)

Figure 27. Rake Face After 28 min. of Cutting (blow-up of Figure 26)

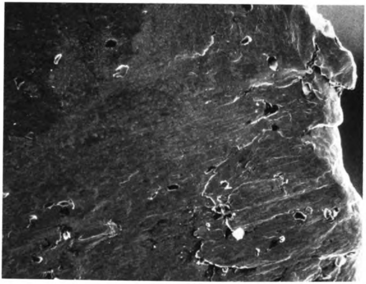

Figure 28. Side Cutting Edge After 29 min. of Cutting

Figure 29. Rake Face After 30 min. of Cutting

5. CORRELATION OF DATA AND SUMMARY OF RESULTS

The results of this study demonstrate that the stress is normally at a maximum near the cutting edge. Even though no exact numerical values for the compressive stress acting within the tool/chip contact area has been determined, the evidence obtained through the finite element analysis illustrates that they are at least high enough to significantly deform the tool tip and side cutting edge. The extent of this deformation is very likely to be larger with the softening effect the temperatures on the tool material. Although classified as a sliding wear pattern, the cratering effect in Figure 23 can very well be caused by the combined effect of sliding, high compressive stresses and fatigue on the rake surface. High temperatures would only accelerate this mechanism. Considering the interrupted nature of turning experiments, a low cycle fatigue loading of the tool might have taken place. The collapse of the tool tip towards the end of the tool life, the crumbling effect seen in Figure 28 and the crack in the destroyed tool in Figure 29 have, besides the discussed mechanisms, very likely been caused by the continuously increasing stresses and fatigue.

The difficulty inherent to stress calculations at the tool tip is in the determination of the tool/chip contact area. The stress is obtained by dividing the tangential cutting force by this area. This calculation gives only very rough results owing to the fact that the area of the chip/tool interface is inherently impossible to determine. The size of this interface is dependent on what goes on in the flow zone which is not well understood yet, since it cannot be observed directly and is governed by several parameters. These experiments, through electron microscopic examination of tool wear, also showed that the seizure between the work material and tool is the normal condition to be expected.

The dependence of tool wear on cutting time and cutting speed gas been one of the major areas of research starting with Taylor's tool life tests around the turn of the century. It is well established that tool life decreases with increasing cutting time and cutting velocity in a progrssive exponential manner. The results of the study are in line with this existing knowledge.

Although the effects of temperature on wear have been excluded from consideration, it was expected that they would be limited under the cutting conditions selected. This assumption was confirmed by the types of wear observed, i.e. abrasion, attrition, wear under sliding conditions, which characteristically occur at low temperatures.

6.DISCUSSION

This study set out to investigate the feasibilty of correlating tool wear to cutting forces and stresses. The idea was to understand the underlying difficulties as well as to discover hidden potentials with a long term goal of on-line monitoring of tool wear on the production level. Much effort has been and is being spent to increase the productivity on the shop floor. The recent developments in Numerical Control (NC), Direct Numerical Control (DNC), and Computer Numerical Control (CNC), although enormous in their positive impact on productivity, can only reduce the non-productive time in manufacturing, i.e. workpiece handling, setup of the job, lead times, tool changes and operator delays. Although NC has a significant effect on downtime, it can do relatively little to reduce the in-process time compared to a conventional machine tool. The most promising answer in reducing the in-process time lies in the use of Adaptive Control (AC), which determines the proper speeds and/or feeds during machining as a function of variations in such factors as workpiece hardness, cutting depth, air gaps in part geometry, tool wear, and so on. This is a control system that measures certain output process variables such as spindle deflection, force, torque, temperature, vibration amplitude, horse power and tool wear (5,16).

Measurement of forces and wear was the objective of this research. Although this was accomplished by indirect methods, it gave much insight into the problems that lay ahead. Much remains to be learned about the flow zone at the tool/chip interface, the behavior of materials involved at high strain rates and temperatures, the nature and size of the contact area between the tool and the chip and the accurate modeling of the tool tip.

LIST OF REFERENCES

1. Oberg, E., Jones, D. F., Horton, H., L., Machinery's Handbook, Industrial Press, Inc., 21st ed., 1980.

2. Metal Cutting Tool Handbook, Metal Cutting Tool Institute, 1954, Hildreth Press.

3. Machining Data Handbook, Metcut Research Associates, Inc., Cincinnati, Ohio, 2nd ed., 1972.

4. "Life Tests on Single-Point Tools", American Standards Association, ASA B5.19-1946, ASA B5-13-1939.

5. Trent, E., M., Metal Cutting, Butterworth & Co., 1977.

6. Childs, T. H., C., Richings, D., Wilcox, A., B., "Metal Cutting: Mechanics, Surface Physics and Metallurgy", International Journal of Mechanical Sciences, Vol. 14, 1972, pg. 359/375.

7. Usui, E., Hirota, A., Masuko, M., "Analytical Prediction of 3-D Cutting Process", Transactions of the ASME, Vol. 100, 1978, pg. 222.

8. ANSYS, Engineering Analysis System, User's Manual, Swanson Analysis Systems, Inc., Houston, Pennsylvania.

9. Zorev, N., N., International Research in Production Engineering, 42, 1963, Pittsburgh.

10. Amini, E., Journal of Strain Analysis, 3, 206, 1968.

11. Zakaria, A., A., ElGomayel, J., I., "On the Reliability of Cutting Temperature for Monitoring Tool Wear", International Journal of Machine Tool Desing,Vol. 15, 1975, pg. 195/208.

12. Tseng, M., M., Noujaim, R., A., "On the Measurement and Propagation of Flank Wear in Cutting Tools", Journal of Engineering for Industry 1979, vol. 101, pg. 109/115.

13. Wright, P., K., McCormick, S., P., Miller, T., R., "Effect of Rake Face Design on Cutting Tool Temperature Distributions", Journal of Engineering for Industry, 1980, Vol. 102, pg. 123/128.

14. Bhattacharyya, A., Ham, I., "Analysis of Tool Wear, Part 1: Theoretical Models of Flank Wear", Journal of Engineering for Industry, 1969, pg. 790/798.

15. Opitz, H., Konig, H., "On the Wear of Cutting Tools", Advances in Machine Tool Design and Research, 1967, pg. 173/200.

16. Groover, M., P., Automation, Production Systems and Computer-Aided Manufacturing, Prentice Hall, Inc., 1980.